

USE OF CFD TO CALCULATE THE DYNAMIC RESISTIVE END CORRECTION FOR MICROPERFORATED MATERIALS

J. Stuart Bolton and Nicholas Kim

Ray W. Herrick Laboratories, Purdue University, West Lafayette In, USA

The classical Maa theory for microperforated materials was initially formulated for constant diameter, cylindrical holes. Since then, a number of *ad hoc* corrections have been suggested to account for different hole shapes: in particular, rounding of the aperture. Here it is shown that the resistance and reactance of small apertures may be calculated using relatively simple CFD models in which a single hole is modelled. The fluid is assumed to be viscous but incompressible, and the geometry is assumed to be axisymmetric. It will be shown that this approach essentially reproduces the classical theory of Maa for circular, sharp-edged apertures. However, it will also be shown that the resistive end correction, in particular, exhibits a clear dependence on frequency and geometrical parameters that is neglected in conventional microperforated material models.

INTRODUCTION

Microperforated materials are of current interest since they provide a useful alternative to fibrous materials in a number of noise control situations. Thus it is important to be able to calculate the acoustical properties of microperforated materials accurately. The best-known model for microperforated materials is that of Maa [1], which is based on a model of oscillatory, viscous flow in small tubes. The Maa model also features end corrections to account for inertial and resistive effects associated with flow converging into the holes. Those corrections have usually been based on a combination of physical reasoning and *ad hoc* comparisons between measured and predicted results. In the present work, an alternative approach has been adopted. Here a simple computational fluid dynamics (CFD) model of oscillatory, viscous flow through a single hole has been developed, and has been used to calculate the specific acoustic impedance of a microperforated sheet. In particular, the emphasis has been placed on the real part of the specific acoustic impedance (here referred to as the dynamic flow resistance) since the energy dissipation produced by a microperforated panel is proportional to that component of the impedance. It will be shown that the CFD results for the dynamic flow resistance are in generally good agreement with the predictions of existing models, particularly at high frequencies, but that they differ significantly at low frequencies. It is suggested that the latter discrepancy results from the neglect of a static, resistive end correction in conventional microperforated material models. Based on the CFD results, a revised dynamic resistive end correction is proposed. Note finally, that only sharp-edged holes have been considered in the present work, but that the general approach can easily be extended to calculate the specific acoustic impedance of microperforated materials having arbitrary hole geometries.

REVIEW OF THEORY

The Maa [1] model can be separated into two parts, one being a linear component and the other a non-linear component which becomes significant at high incident sound pressure levels. In this study, the focus is on the linear part, only. The linear component of the Maa model is derived from Rayleigh's [2] formulation for wave propagation in narrow tubes. Based on those equations, Crandall [3] modeled dissipation in small diameter channels, and Maa further developed Crandall's model for the case of very small holes in which the oscillatory viscous boundary layer spans the hole diameter. For a circular-hole model, the equation for the normal specific acoustic transfer impedance of a microperforated sheet (without end correction) is expressed as:

$$Z = \frac{j\omega t}{\sigma c} \left[1 - \frac{2}{k\sqrt{-j}} \frac{J_1(k\sqrt{-j})}{J_0(k\sqrt{-j})} \right]^{-1} \quad (1)$$

where ω is the angular frequency, t is a length of the hole (usually the same as the thickness of the perforated sheet), c is the speed of sound, σ is the surface porosity of the sheet (i.e., the fraction of the total surface area occupied by holes), k is the perforation constant defined by $k = d\sqrt{\omega\rho/4\eta}$, η is the dynamic viscosity, ρ is the air density, d is the hole diameter, and J_0 and J_1 are the Bessel functions of the first kind of zeroth and first order, respectively.

A resistive end correction was suggested by Ingard [4], to account for energy dissipation at the surface of the sheet as flow approaches the hole. Ingard called this effect a surface resistance, and the surface resistance on one side of the hole was defined as $R_s = \frac{1}{2}\sqrt{2\eta\rho\omega}$. In the microperforated panel formulation of Guo *et al.* [5], the end correction is added to the real part of the above expression as:

$$r = \text{Re} \left\{ \frac{j\omega t}{\sigma c} \left[1 - \frac{2}{k\sqrt{-j}} \frac{J_1(k\sqrt{-j})}{J_0(k\sqrt{-j})} \right]^{-1} \right\} + \frac{\alpha 2R_s}{\sigma\rho c} \quad (2)$$

where r is the real part of the specific acoustic transfer

impedance, R_s is the surface resistance, and α is a nominally frequency-independent factor which accounts for hole type. It was suggested by Guo *et al.*, based on a comparison with measurements, that α should be set to 4 when the hole is sharp-edged, and should be set to 2 when the hole has a rounded edge. Maa also used the surface resistance for the end correction, but he did not include a factor to account for hole shape.

In the present work, it has been found that the value of α in the above formulation is not necessarily independent of frequency. The objective here is to introduce a numerical procedure to identify the value of α that makes Eq. (2) exact for a given hole geometry.

CFD MODEL OF AN ORIFICE

Geometry

To perform the CFD calculations, it was first necessary to create a discretized model of a single, sharp-edged hole, and a corresponding channel. The microperforated panel was modeled geometrically using the software Gambit. The models were classified into 3 groups: one was a group having different panel thicknesses; the second was a group having different hole diameters; and the last was a group having different surface porosities. The mesh interval was chosen to be 0.005 mm in order to ensure accurate results for the smallest hole considered. In addition, the model was made axisymmetric (i.e., two-dimensional) to make the calculation time relatively short. Figure 1 shows the basic perforated panel model. Note that in Fig. 1, the bottom of the figure represents the center-line of the axisymmetric model.

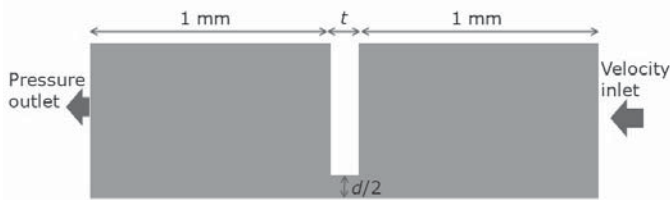


Figure 1. The geometry of the CFD model for a microperforated panel.

CFD Parameters

The CFD calculations were performed by using the commercial software Fluent. Since all model dimensions were very small compared to a wavelength at all frequencies of interest, the flow was assumed to be incompressible, and as a result there was no energy loss by heat transfer. The simulation was a pressure-based, implicit formulation, the Green-Gauss node-based method was selected for the gradient option, and the second-order implicit method was chosen for the unsteady formulation. The options selected were: SIMPLE for the pressure-velocity coupling method, STANDARD for pressure, and SECOND-ORDER UPWIND for momentum. The outlet pressure was set to ambient pressure, and the inlet velocity was chosen to be a Hann windowed, 5 kHz half-sine wave having a maximum value of 1 mm/s in order to cover the frequency range up to 10 kHz. The simulations were run for 200 time

steps over a period of 0.1 ms, and the time interval was chosen to be 0.5 μ s. The imposed inlet velocity and the resulting inlet pressure for one case are shown in Fig. 2(a), while the spectra of the inlet velocity and pressure are shown in Fig. 2(b). Note that zero tangential velocity boundary conditions were imposed in the hole and on the surface of the plate section, but not at the outer surfaces of the inlet and outlet channel sections. As mentioned above, three sets of models were considered in which the following parameters were changed: panel thickness; hole diameter; and surface porosity. The specific parameters for the three models sets are listed in Table 1.

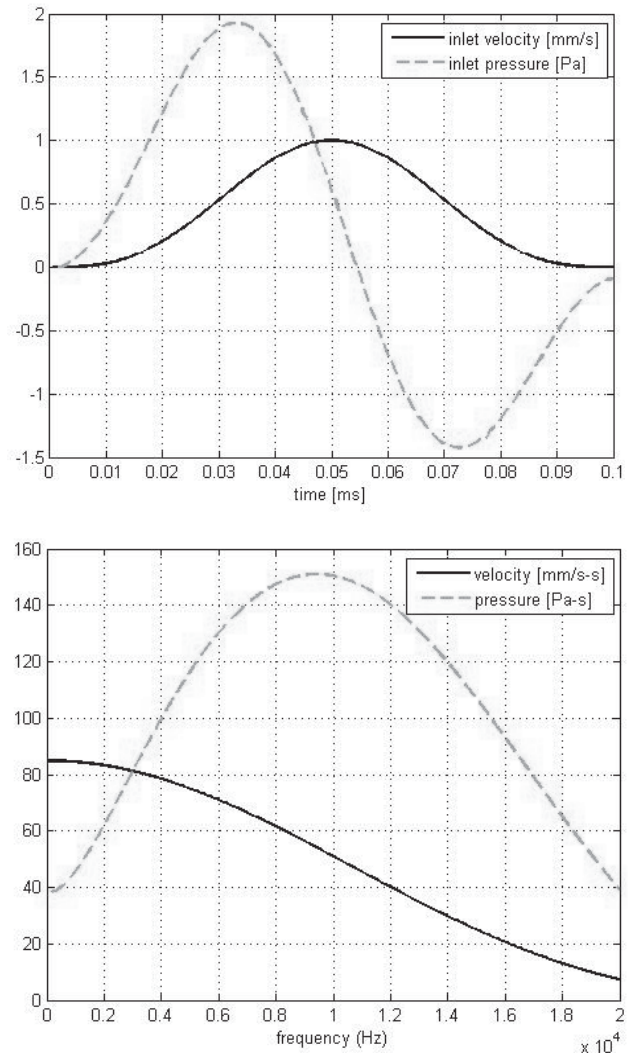


Figure 2. (a) Inlet velocity and pressure vs. time (b) Inlet velocity and pressure magnitude vs. frequency ($t = 0.4064$ mm, $d = 0.2032$ mm, $\sigma = 0.02$).

Table 1. Parameters of three model sets (t is thickness, d is diameter of the hole, σ is the surface porosity).

Set 1. Thickness			Set 2. Diameter			Set 3. Porosity		
t (mm)	d (mm)	σ	t (mm)	d (mm)	σ	t (mm)	d (mm)	σ
0.1016	0.4064	0.02	0.4064	0.1016	0.02	0.4064	0.2032	0.005
0.2032	0.4064	0.02	0.4064	0.2032	0.02	0.4064	0.2032	0.01
0.3048	0.4064	0.02	0.4064	0.3048	0.02	0.4064	0.2032	0.015
0.4064	0.4064	0.02	0.4064	0.4064	0.02	0.4064	0.2032	0.02
0.508	0.4064	0.02	0.4064	0.508	0.02	0.4064	0.2032	0.025
0.6096	0.4064	0.02	0.4064	0.6096	0.02	0.4064	0.2032	0.03
0.7112	0.4064	0.02				0.4064	0.2032	0.035
0.8128	0.4064	0.02				0.4064	0.2032	0.04
0.9144	0.4064	0.02						

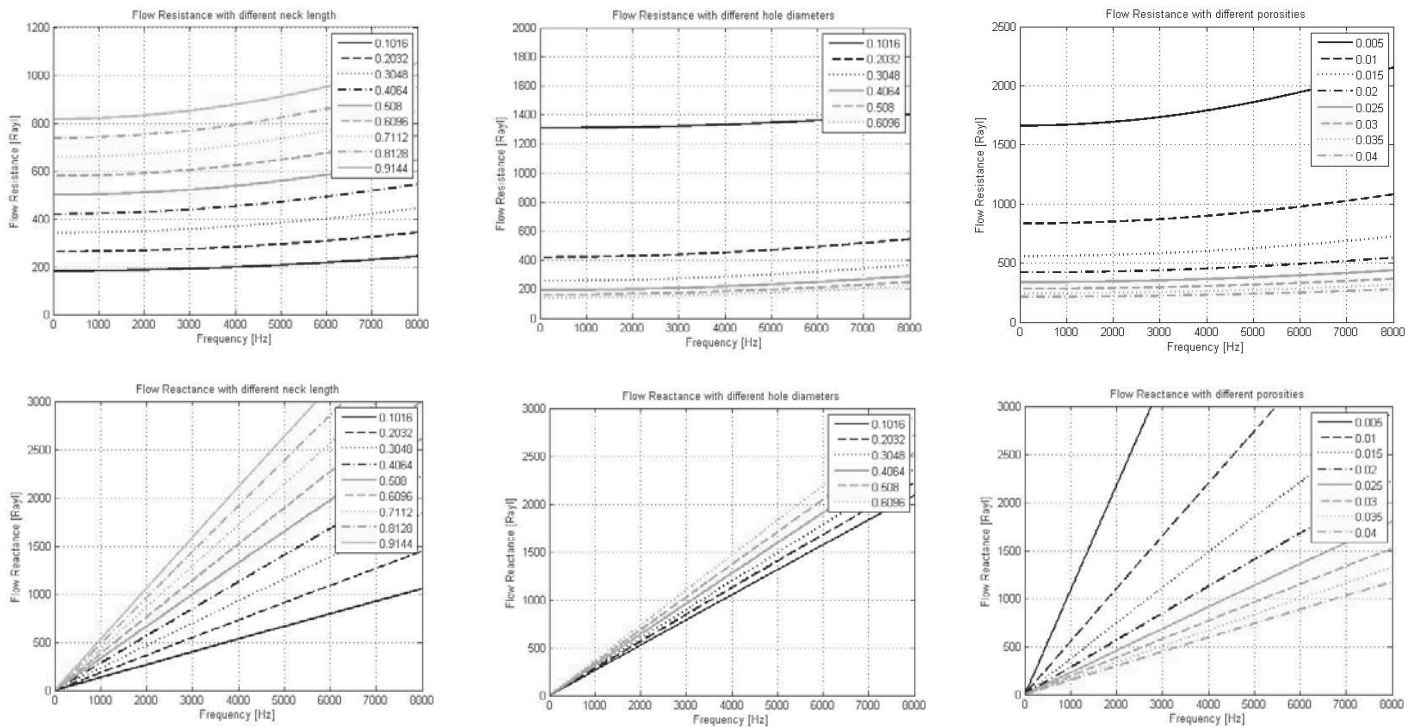


Figure 3. Dynamic flow resistance and dynamic flow reactance of set 1 (left), set 2 (middle), and set 3 (right).

Transfer Impedance

The specific acoustic transfer impedance of the panel was calculated as $Z = (P_1 - P_2)/V$. Here, P_1 is the inlet pressure, P_2 is the outlet pressure (which is the ambient pressure), and V is the inlet velocity; all of these quantities were Fourier transformed in order to obtain the impedance in the frequency-domain. The real part of the specific impedance is referred to here as the dynamic flow resistance, and the imaginary part is referred to as the dynamic flow reactance. Figure 3 shows the flow resistance and flow reactance for the three model sets described above.

As expected, the dynamic flow resistance increases as the thickness increases, the diameter decreases, or the porosity decreases. The dynamic flow reactance, which will not be considered in detail here, shows a pure mass-like characteristic, as expected. To illustrate the difference between the CFD results and the predictions of the Guo *et al.* model, one particular case is considered here: the thickness of panel was 0.1016 mm, the hole diameter was 0.1016 mm, and the porosity was 0.02. In the Guo *et al.* model, the parameter α was set to both 2 (round-edged hole) and 4 (square-edged hole), for the purpose of illustration. The comparison of the impedances is shown in Fig. 4, and Fig. 5 shows the absorption coefficients of the microperforated material for various backing depths calculated by using both CFD-based impedance and the Guo *et al.* model (with $\alpha = 2$). The surface normal impedance of the microperforated sheet and a rigidly terminated air spaces was calculated as $z_p = -j\rho c \cot k_a L$, where k_a is the wave number in air (ω/c), and L is the air layer depth. The normal incidence plane wave reflection coefficient is then $R = \frac{(z_p - \rho c)}{(z_p + \rho c)}$ and the normal incidence absorption coefficient is $\alpha_n = 1 - |R|^2$.

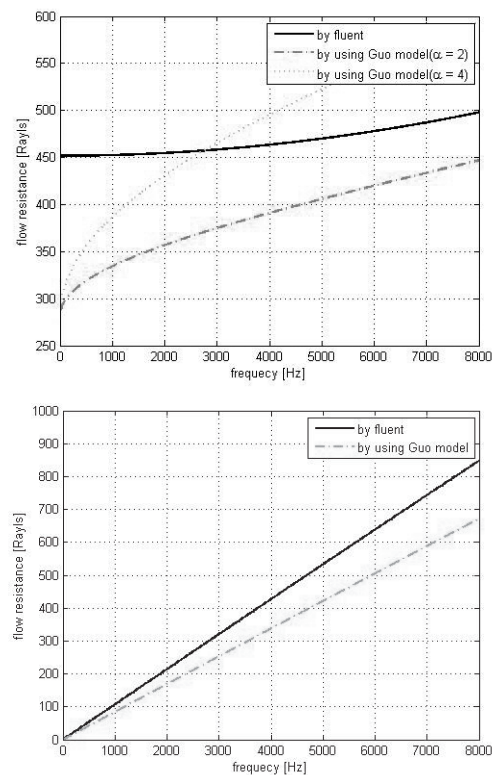


Figure 4. Dynamic flow resistance (top) and flow reactance (bottom) at $t = 0.1016$ mm, $d = 0.1016$ mm, $\sigma = 0.02$.

The dynamic flow resistance calculated from the CFD simulations generally lies between those predicted by the Guo *et al.* model for $\alpha = 2$ and $\alpha = 4$; the CFD reactance is very similar in character but slightly larger. The CFD and

Guo *et al.* flow resistances differ most significantly in the low frequency range. It is suggested that the difference in the dynamic flow resistance at low frequencies results from the neglect of a static, resistive end correction in conventional microperforated material models. The resistive contribution to the hole impedance from flow over surfaces adjacent to the hole (and from shearing within the fluid exterior to the hole as flow converges into the hole) does not vanish at 0 Hz: i.e., under steady flow conditions. However, the assumed frequency dependence of the resistive end correction in the Guo *et al.* model (and in the Maa model on which it is based) necessarily causes the resistive end correction to become

negligible at low frequencies (when the parameter α is assumed to be frequency-independent). This effect is believed to be primarily responsible for the difference between the Guo *et al.* and related models and the present CFD results, and this is the major finding of the current work. Since the major difference between the Guo *et al.* impedance predictions and those made using the present approach are in the dynamic flow resistance, the magnitudes of the absorption coefficients predicted using the two approaches will differ in the low frequency range but the peak locations (determined by the dynamic flow reactance) will be approximately the same: this behaviour is illustrated in Fig. 5.

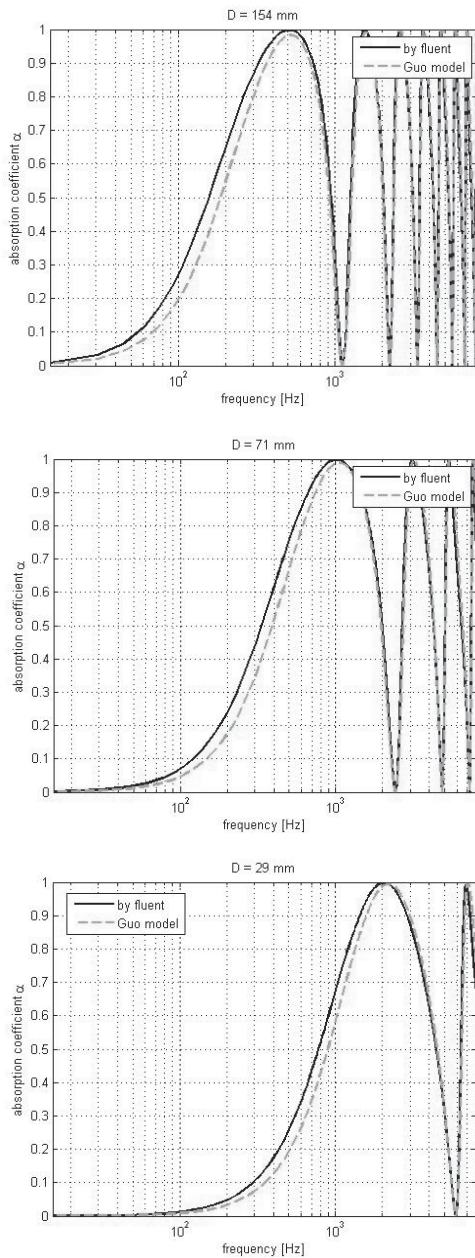


Figure 5. Comparison the absorption coefficient of a microperforated sheet ($t = 0.1016$ mm, $d = 0.1016$ mm, $\sigma = 0.02$) with air backing ($L = 154$ mm, $L = 71$ mm, $L = 29$ mm).

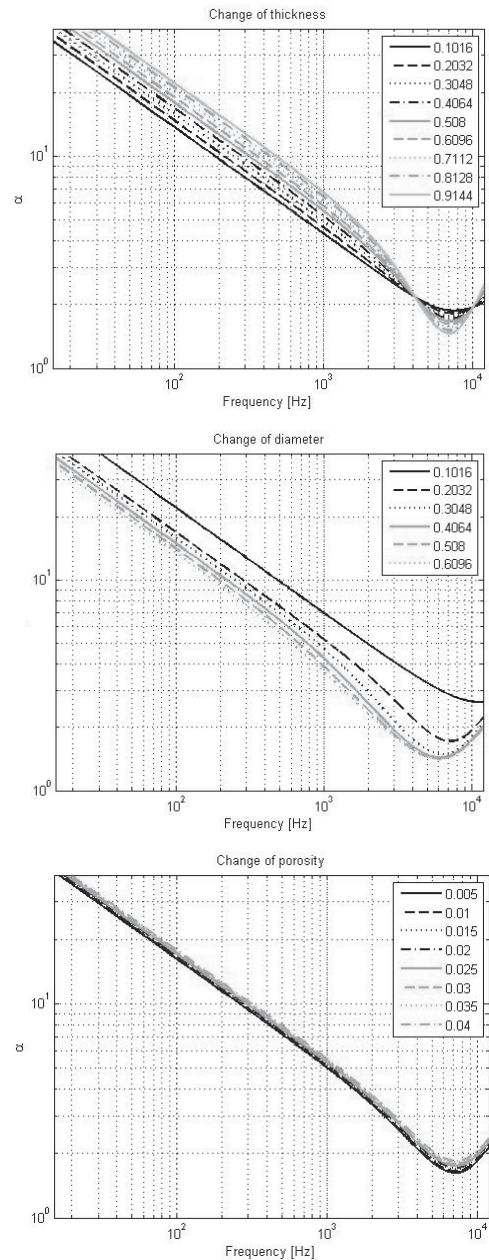


Figure 6. α vs. frequency for different thicknesses (top), different hole diameters (middle), and different surface porosities (bottom).

DYNAMIC RESISTIVE END CORRECTION

As noted above, the difference between the Guo *et al.* model and the CFD simulations results primarily from the resistive end correction. The end correction in the Guo *et al.* model is expressed as $\frac{\alpha 2R_s}{\sigma \rho c}$, where α equals 4 for a sharp-edged hole. To improve the accuracy of the Guo *et al.* model, it would be necessary to make the parameter α dependent on frequency (as well as on the hole geometry and surface porosity). Here, the value of α has been calculated that would be required to force perfect agreement between the Guo *et al.* model (for the specific resistance) and the CFD results. Figure 6 shows the dependence of α on frequency and on geometric parameters, when defined in this way.

From Fig. 6 can be seen that α is generally inversely proportional to frequency in the low frequency region, but that it appears to be approaching a constant value at high frequencies. The results in Fig. 6 also indicate that as the panel thickness increases, the value of α also increases. In the same way, the value of α increases as hole diameter decreases. In the variable porosity cases, the porosity does not have a strong effect in the range considered here. These results imply that α should, in principle, be treated as a function of frequency, thickness, hole diameter, and porosity. In the Fig. 6, all three graphs show that α is approximately proportional to $f^{-0.5}$. Therefore, α can be conveniently represented as:

$$\alpha = \beta f^{-0.5} \quad (3)$$

Then, a new parameter β , is defined to be a function of thickness, hole diameter, and porosity. Figure 7 shows β for different thicknesses, hole diameters, and porosities at 5 kHz. Figure 7 implies that β is proportional to porosity, and inversely proportional to thickness and hole diameter. Based on the change of dynamic flow resistance at 5 kHz, an approximate expression for the parameter β , as a function of thickness, hole diameter, and porosity, is suggested as:

$$\beta = (14.1 - 0.059 \sigma) \frac{t}{d} + 117 \quad (4)$$

The constants were determined by a least square method. Note that since the porosity is always smaller than 1 (so that 14.1 is always much larger than 0.059σ), under normal circumstances the porosity term can be neglected. The new parameter β is then simply defined as:

$$\beta = 14.1 \frac{t}{d} + 117 \quad (5)$$

Equation (3) shows that α depends on frequency, and Eq. (5) shows that α is function of thickness and hole diameter.

From these results, a new resistive end correction can be defined, based on Guo's end correction but in which the value of α is given as, $\alpha = \beta f^{-0.5}$. Figures 8, 9, and 10 show comparisons of the value of α obtained using the CFD simulations with that predicted using the new parameter β . From these three different cases it can be seen that the suggested form of the parameter β results in reasonable agreement between the CFD results and the approximate predictions over a relatively wide range of hole

parameters. Finally, the absorption coefficients calculated by using the three different methods are plotted in Fig. 11, where it can be seen that the results calculated using the parameter β as defined in Eq. 5 are essentially indistinguishable from those calculated using the CFD-based impedance.

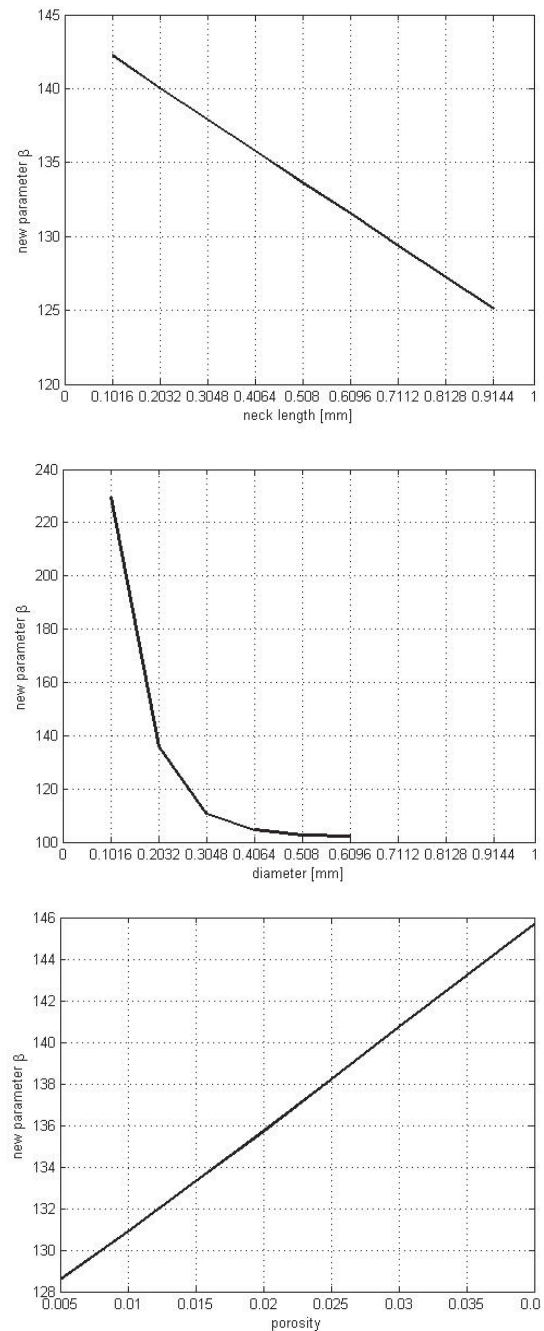


Figure 7. β vs. thickness (top), hole diameter (middle), and porosity (bottom) at 5000 Hz.

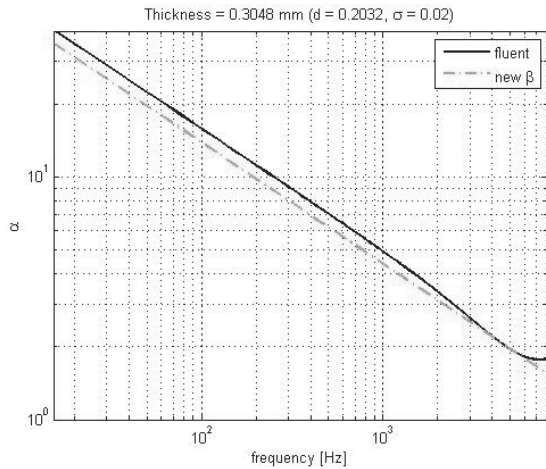


Figure 8. End correction from CFD simulation (solid line) vs. prediction with new parameter β (dash-line) at $t = 0.3048$ mm ($d = 0.2032$ mm, $\sigma = 0.02$).

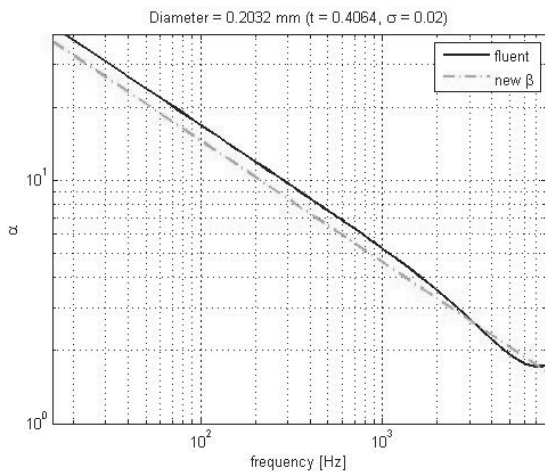


Figure 9. End correction from CFD simulation (solid line) vs. prediction with new parameter β (dash-line) for $d = 0.2032$ mm ($t = 0.4064$ mm, $\sigma = 0.02$).

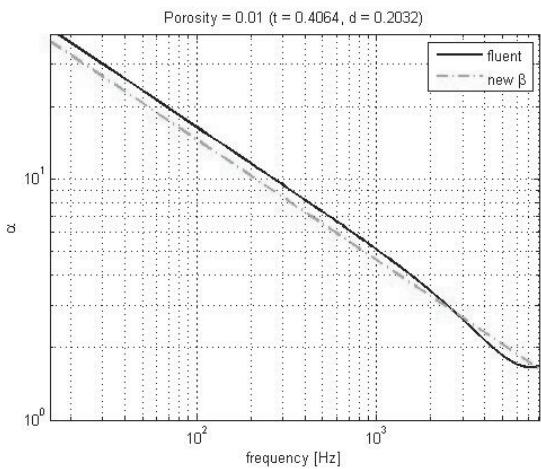


Figure 10. End correction from CFD simulation (solid line) vs. prediction with new parameter β (dash-line) for $\sigma = 0.01$ ($d = 0.2032$ mm, $t = 0.2032$ mm).

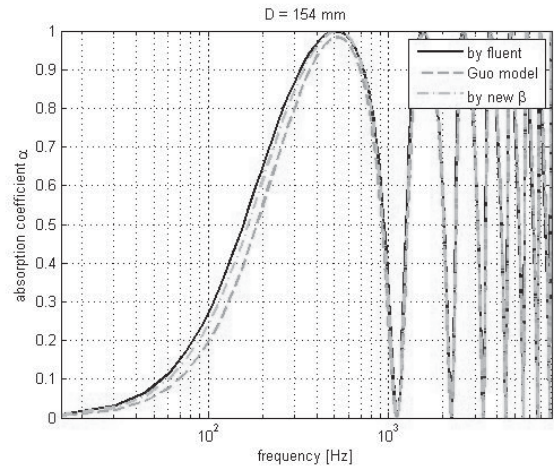


Figure 11. Absorption coefficient calculated by using different impedance values ($L = 154$ mm, $t = 0.1016$ mm, $d = 0.1016$ mm, $\sigma = 0.02$).

CONCLUSIONS

In this paper, CFD models of microperforated materials have been considered. It has been demonstrated that those models generally produce results that conform with well-established theoretical models, but may be more accurate at low frequencies. The CFD models have been used to generate corrections which can be applied to existing models to improve the accuracy of their predictions. Here, only square-edged holes have been considered, but the same approach can easily be extended to other hole geometries. An examination of the effect of varying hole geometry will be the subject of future work.

ACKNOWLEDGMENTS

The authors are grateful to Thomas Herdtle of 3M Corporation, St. Paul, Minnesota, for his useful, practical advice at an early stage of this work. The authors are also grateful to the National Aeronautics and Space Administration who supported this work through the Fundamental Aeronautics Subsonic Fixed Wing project under grant NNX07AV01A (monitor R.J. Silcox).

REFERENCES

- [1] D.Y. Maa. Theory and design of microperforated panel sound-absorbing constructions. *Scientia Sinica* **18**, 1975, 55-71.
- [2] Lord Rayleigh. *Theory of Sound*. McMillan, New York, 2nd edition, 1929.
- [3] I.B. Crandall. *Theory of Vibrating Systems and Sound*. Van Nostrand, New York, 2nd edition, 1926.
- [4] U. Ingard. On the theory and design of acoustics resonators. *Journal of the Acoustical Society of America*. **25**, 1953, 1037-1061
- [5] Y. Guo, S. Allam, and M. Abom. Micro-perforated plates for vehicle applications. *Proceedings of INTER-NOISE 2008*, Shanghai, China, 26-29 October 2008.

NUMERICAL PREDICTION OF THE TRANSMISSION LOSS OF LEAKS IN TRIMMED PANELS

Israel Pereira¹, Marcus Guettler² and Sascha Merz³

¹Universidade Federal de Santa Catarina, Brazil

²Technische Universitaet Dresden, Germany

³ESI US R&D San Diego, USA

Small holes and pass-throughs can often have a significant impact on the transmission loss of trimmed panels, particularly at mid and high frequencies. The effect of such “leaks” can be included in modelling methods such as Statistical Energy Analysis (SEA) by using various analytical leak models. Such models typically assume a simple cross-sectional geometry in order to calculate the leak TL. However, for more complex configurations, for example, where a pass-through only penetrates certain layers of a multi-layer noise control treatment applied to the panel, a more detailed model is required in order to determine the TL of the leak. In this paper, Foam Finite Elements have been used to create such local models in order to predict the TL of partially trimmed pass-throughs. This local TL can then be used to update a system level SEA model. In addition, the paper demonstrates the widely known result that the TL of a simple hole does not depend on its cross-sectional shape but only its cross-sectional area and length. Results are presented for a number of examples.

INTRODUCTION

Statistical Energy Analysis (SEA) is an established numerical method for modelling the response of complex vibro-acoustic systems over a wide frequency range [1, 2]. A common application of SEA is prediction of interior noise in a vehicle due to external acoustic excitation, along with the design of the interior “sound package” of the vehicle [3]. A typical airborne SEA vehicle model is shown in Fig. 1. The model consists of SEA subsystems that represent plates, cavities and semi-infinite fluid domains. The subsystems are coupled via point-, line- and area-junctions (the latter typically contain multi-layer noise control treatments or NCTs). Acoustic excitation is applied to the exterior of the vehicle and interest lies in predicting the sound pressure level in the driver and passenger head spaces. The SEA model also typically contains leaks to represent holes and pass-throughs in the structure and sound package. Such leaks are important for higher frequencies, where they can sometimes become the primary transmission path.

In order to represent simple leaks such as circular and rectangular apertures, analytical representations of the leak TL can be included in the SEA model [4]. However, in some instances a more detailed description of a leak is required, for example, to confirm that a simple leak model can represent a hole with a complex cross-sectional shape or to update an SEA model, where the leak only penetrates through certain layers of a NCT. For either case, only the local transmission loss (TL) of the leak is needed. This can be computed using a detailed numerical model and used to update a system level SEA model.

This paper presents numerical results for the TL of various leaks. The impact of cross-sectional shape is investigated, for leaks with the same length and cross-sectional area. The influence of sound package on the TL of a leak is then analysed

and results for various local models of the leak are discussed. In order to cover a broad frequency range, the Hybrid FE-SEA method [5-7] has been used to perform the numerical simulations in this paper. In these models acoustic finite elements have been used to model the fluid in the local vicinity of the leak. The noise control treatment has been modelled using Foam Finite Elements [7, 8] based on Biot theory and the acoustic half-space on either side of the panel is represented by SEA acoustic fluids. It has been assumed that for the frequency range of interest (i) leak TL is dominated by local properties and (ii) edge effects are negligible. All models have been created in the commercial software package VA One [7].

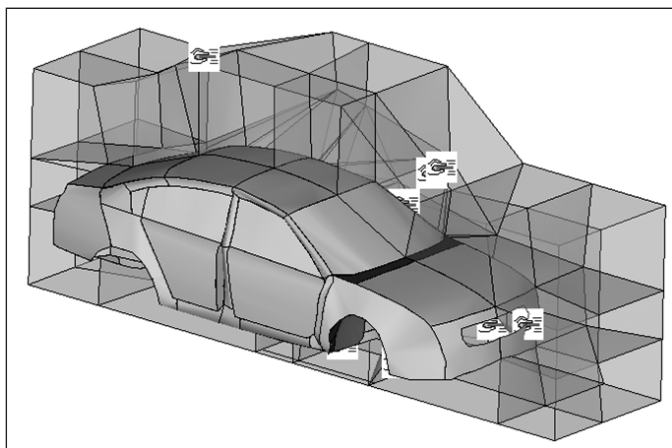


Figure 1. Typical vehicle airborne SEA model.

PREVIOUS STUDIES

A study of the transmission loss of slits and seals for airborne SEA was recently conducted by Cordioli *et al.* [9]. In this work the TL of an automotive door seal was investigated using Hybrid FE-SEA models. It was found that the inclusion of the acoustic “channel” before and after the seal can have a significant impact on the overall TL of the seal. It was also shown that for “slits” a Hybrid FE-SEA model provided a quick way to model the slit TL and that the geometrical complexity of the channel does not have a significant impact on the TL of the slit (the TL scales with the overall length and cross-sectional area of the channel). The current paper uses a similar modelling approach but applied to trimmed pass-throughs.

INFLUENCE OF ACOUSTIC LEAK ON THE TL OF A TRIMMED PANEL

This section provides a simple example of the influence of a leak on the TL of a simple panel. Consider a 1mm thick steel plate between two air filled cavities shown in Fig. 2. A noise control treatment layup consisting of 20mm melamine foam and a 1.5kg/m² septum has been applied to the steel plate. A circular leak with a diameter of 10mm diameter is added to the steel plate using an analytical formulation [4]. An SEA model of the system is created that contains two cavity subsystems (with overridden volumes to simulate large reverberant rooms), one plate subsystem and the leak in the area junction between the panel and the cavities.

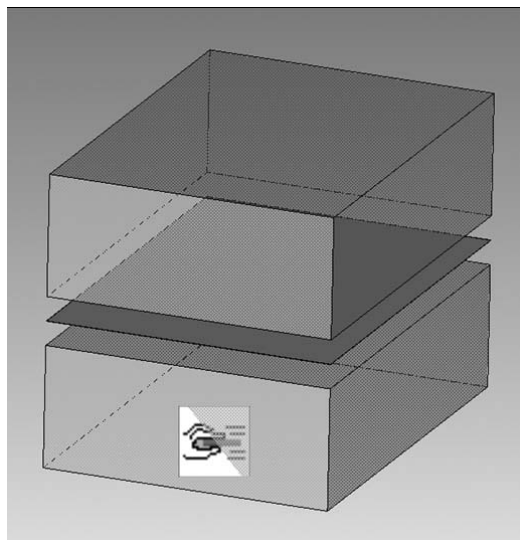


Figure 2. SEA model used to predict TL through a steel plate of dimension 1.64m×1.19m×0.001m with a NCT layup consisting of 20mm of melamine foam, a 1.5kg/m² septum and a 10mm diameter “leak”.

The predicted TL results are shown in Fig. 3 for four configurations of bare and trimmed panels with and without a leak. It can be seen that, for this model, the leak is the dominant transmission path above approximately 1 kHz when the panel is trimmed. This is not the case with the bare panel where the ‘weak’ path is still the panel itself. The TL curve for a different

leak (with 30mm depth and 10mm diameter) is plotted in Fig. 4. The curve can be used to show typical characteristics of the leak TL. Below approximately 1kHz the TL of the leak is fairly constant and is determined by “aperture” effects. Above approximately 10kHz the local TL of the leak tends to zero and the TL is determined by the “area” of the leak (the TL tends to approximately 44dB in this example since the TL is normalized to the overall area of the panel). Between 1kHz and 10kHz various local acoustic resonances of the leak occur.

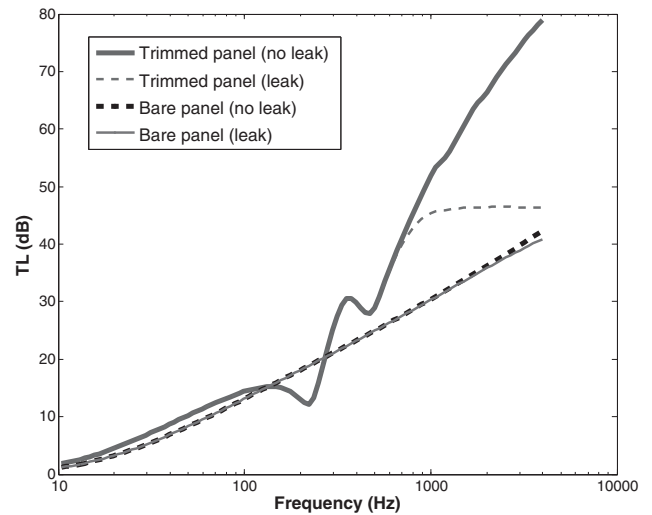


Figure 3. Influence of a leak on the TL of bare and trimmed panels.

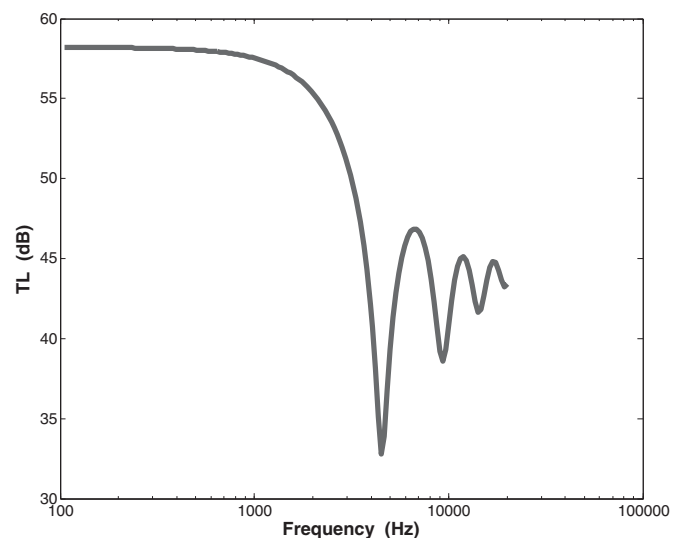


Figure 4. Transmission loss (normalized to panel area) for a rigid panel with a single circular pass-through having 10mm diameter and 30mm depth.

INFLUENCE OF CROSS-SECTIONAL SHAPE ON UNTRIMMED LEAK

The previous examples considered a leak with a simple cross-sectional geometry modelled analytically. This section considers the TL of leaks with more complex cross-sectional shapes. The leaks shown in Fig. 5 were selected; each has

the same depth and cross-sectional area but different cross-sectional shapes. Various Hybrid FE-SEA models were created for the leaks as shown in Fig. 6. The leaks are represented by Acoustic Finite Elements (this allows any leak geometry to be investigated, including situations in which the cross-sectional area of the leak varies throughout the depth of the leak). The Acoustic FE subsystems are then connected to SEA semi-infinite fluids (SIFs) using “Hybrid Area Junctions”. A “baffled” boundary condition option was selected for these Hybrid Area Junctions. Each SIF then describe a (complex and full) radiation impedance looking into a baffled half space. A diffuse acoustic field was applied to the source side (the DAF is represented by a reciprocity relationship as discussed in [10]). The advantage of the Hybrid FE-SEA models is that they solve very quickly (the models in this example solved in a matter of seconds).

The TL predicted by the various Hybrid models and the TL predicted for a circular leak by an analytical model are shown in Fig. 7. It can be seen that the TL curves are almost identical, highlighting that (for frequencies at which the wavelength is large compared with the dimension of the leak) the TL is insensitive to the cross-sectional shape of the leak. There is close agreement between the Hybrid result and analytical results (the small differences are perhaps due to the simplifying assumption adopted in the analytical model that the pressure within the leak is uniform across the leak cross-section). The results in this section are consistent with the standard SEA practice of using a simplified leak formulation to describe leaks with different cross-section.

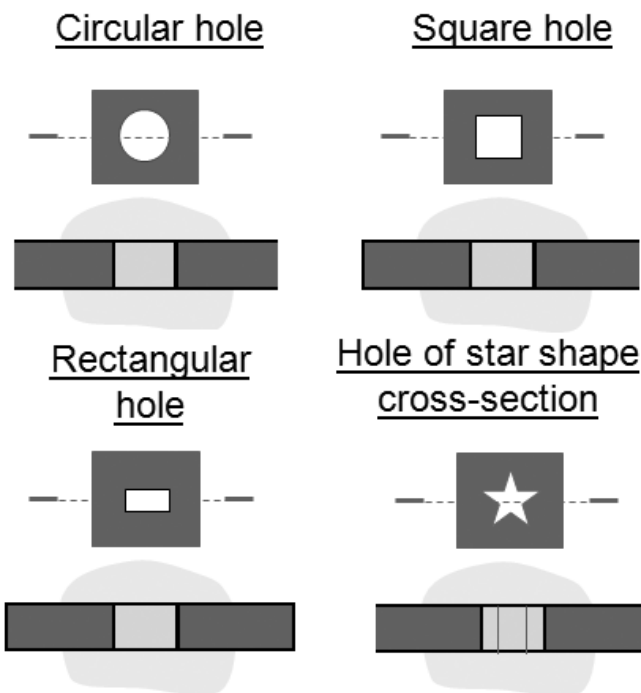


Figure 5. Examples for pass-throughs having simple and complex cross-sectional shape.

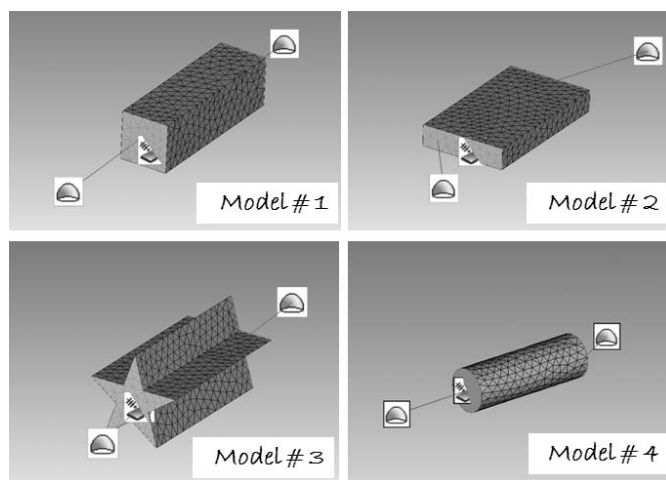


Figure 6. Hybrid FE-SEA models of leaks with the same cross-sectional area and depth but different cross-sectional shapes.

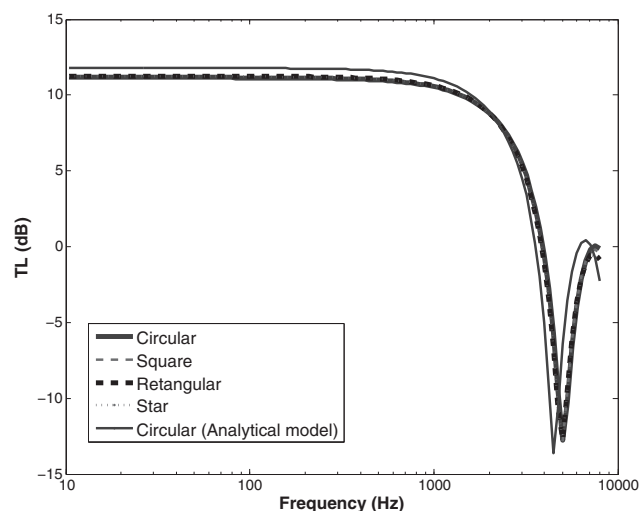


Figure 7. TL of leaks with different cross-sectional shape using a Hybrid FE-SEA model and of a circular leak using an analytical model.

MODELLING A TRIMMED LEAK: FULL PANEL MODEL

Consider now the problem of applying a layered noise control treatment over a given leak. In principle, a model could be created in which the panel is modelled in detail using Structural Finite Elements, the trim modelled with Foam Finite Elements and SEA fluids applied to either side to model the TL. This is investigated in the current section.

A Hybrid model of the previous flat trimmed panel has been developed using foam finite elements to represent the trim and structural finite elements to represent the panel. The air is modelled using SEA semi-infinite fluids on either side of the panel. 700 structural modes have been extracted to represent the response of the steel panel. The foam is represented by approximately 70,000 foam finite elements. The model is shown in Fig. 8. Results for the same configuration have also been obtained using an SEA model, where the air is represented

by SEA acoustic cavities, the panel is represented by an SEA plate and the trim is described with the standard SEA transfer matrix approach for poroelastic layups. For the Hybrid FE-SEA model, a frequency range from 10 to 1,000Hz has been considered, where 80 frequency points were computed. For the pure SEA model, a frequency range from 100 to 5,000Hz has been investigated. On a 4 core 64-bit machine with 2.2GHz clock frequency and 8GB of RAM, the detailed Hybrid model required approximately 70 hours to solve, whereas the simple SEA model required 5 seconds. The majority of the computational expense of the Hybrid model was associated with the explicit representation of the trim using foam finite elements (the computational time may be reduced through the use of frequency interpolation but this was not employed in the current example).

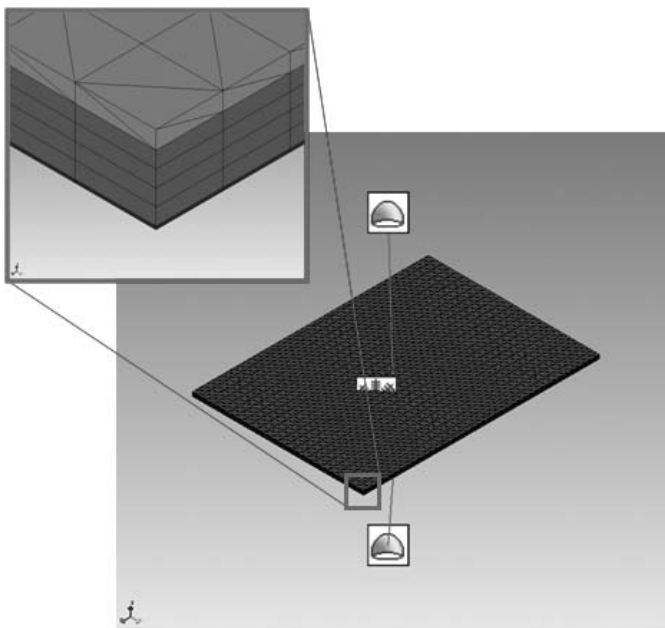


Figure 8. Hybrid FE-SEA-PEM model of a trimmed panel.

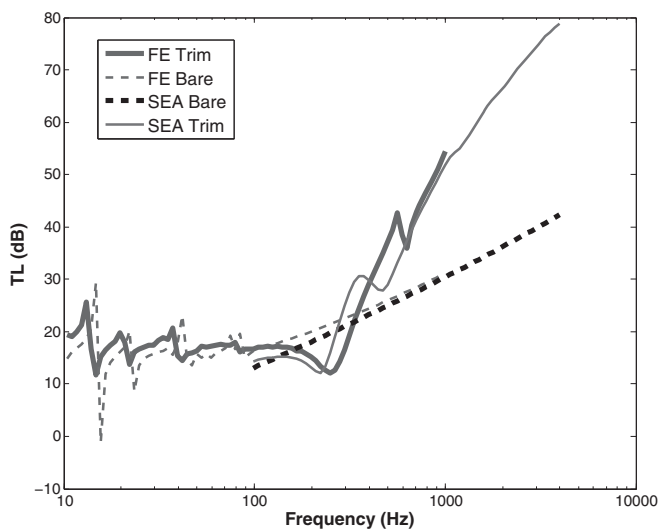


Figure 9. Comparison of the transmission loss obtained from pure SEA and Hybrid FE-SEA-PEM models for an untrimmed and a trimmed panel.

The results for the TL of the trimmed and untrimmed panels are presented in Fig. 9. The models are in close agreement across the common frequency range. However, the example highlights that the use of a detailed finite element model of the entire panel may result in long solve times which may not be practical for quick design studies. It is therefore natural to question whether a detailed model of an entire panel is needed in order to assess the TL of a trimmed leak. The following sections investigate this in more detail.

MODELLING A TRIMMED LEAK: LOCAL MODELS

An alternative approach to modelling an entire panel is to create a local model of a leak that includes the trim in the “local” vicinity of the leak. A question that then arises is “*how much of the surrounding trim do I need to include in a local model to characterise the effect of the trim on a given leak?*”. In this section this question is addressed by comparing the results from two different Hybrid models of a trimmed leak. The models are used to assess the sensitivity of the TL to the amount of foam that is modelled.

The Hybrid models are shown in Figs. 10 and 11. The leak is modelled with acoustic finite elements as before. The foam and septum in the vicinity of the leak are modelled with foam finite elements. SEA SIFs are then added to model the source and receiving sides of the leak. The difference between the two Hybrid models is that the first model is larger than the second model (the first model includes a larger cross-sectional area than the second model).

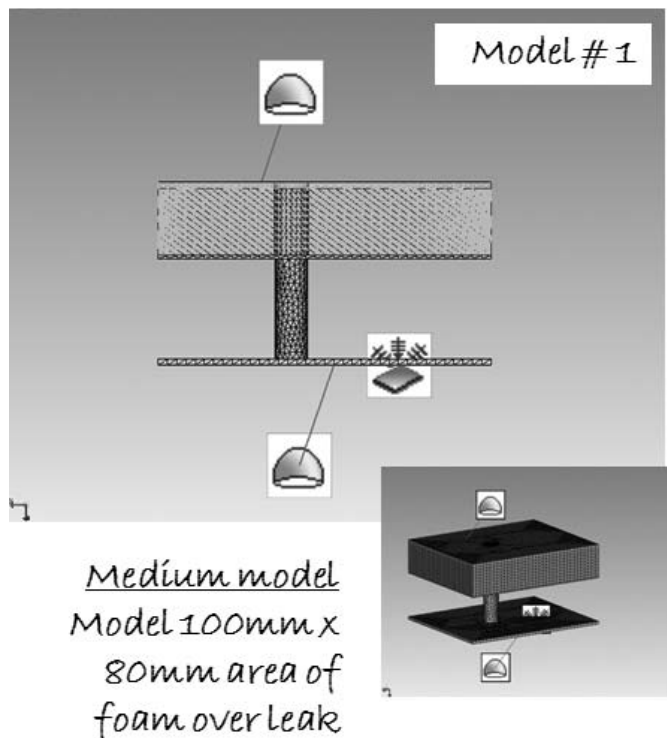


Figure 10. Hybrid FE-SEA model of trimmed leak (medium sized model).

For the two models, the dimensions of the cut-out were chosen to be 100mm×80mm and 50mm×30mm, respectively. The TL from both models is presented in Fig. 12 along with the TL of an “untrimmed” leak. It can be seen that, for this model, above approximately 300 Hz the results from the two models are identical. Below 300 Hz the results are sensitive to finite size effects and the TL depends on the boundary conditions applied to the edge of the foam. At first sight this might suggest that it is necessary to use a larger model to characterize the insertion loss that the treatment applies to the leak TL. However, as discussed in previous sections, the TL of a leak is often dominant at higher frequencies. In such instances it may therefore be possible to use a local Hybrid FE-SEA model to characterize the insertion loss that the trim applies to the leak.

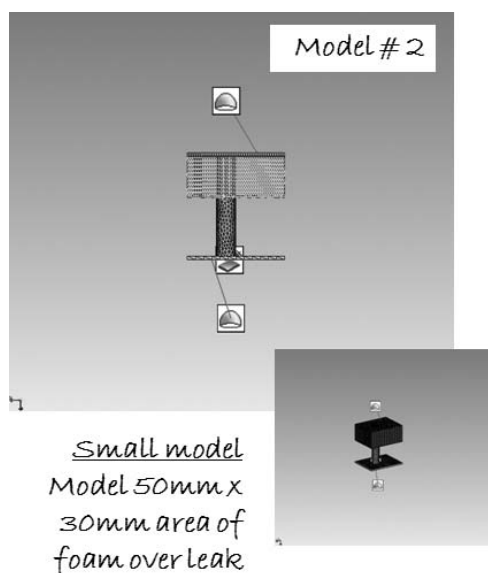


Figure 11. Hybrid FE-SEA model of trimmed leak (small model).

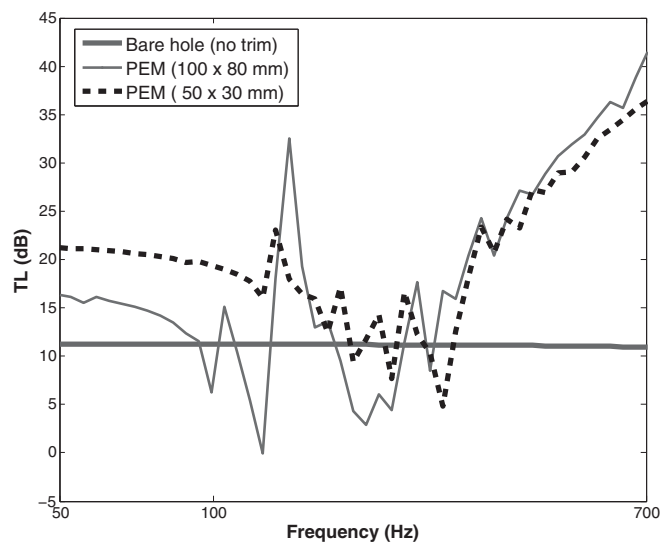


Figure 12. Comparison of the TL of a trimmed leak predicted by Hybrid models (frequencies over 300 Hz of interest for typical leak).

CONCLUSIONS

This paper has presented a number of methods for creating detailed local models of leaks. The main application of the current work is updating system level SEA models with information from detailed local Hybrid FE-SEA-PEM models. It was demonstrated that (at lower frequencies) the TL of an untrimmed leak is insensitive to cross-sectional shape and only depends on overall cross-sectional area and depth. The use of local Hybrid FE-SEA-PEM models was then investigated for modelling the TL of a trimmed leak. For the configurations in the current paper the use of smaller local models provided similar estimates of TL at higher frequencies indicating that it is not necessary to model an entire panel in order to characterize the TL of a trimmed leak. While the current paper focused on simple trim layouts, the proposed approach is expected to be applicable to more complex layouts involving partial coverage and complex cut-outs within the treatment.

ACKNOWLEDGEMENTS

This work was performed while the first and second authors were research interns at ESI US R&D. Helpful discussions with Vincent Cotoni and Phil Shorter are acknowledged. All models discussed in the current paper were developed using the commercial vibro-acoustics software VA One [7].

REFERENCES

- [1] R.H. Lyon and R.G. DeJong, *Theory and Application of Statistical Energy Analysis*, Butterworth-Heinemann, Newton, MA, 1995
- [2] R.J.M. Craik, *Sound Transmission through Buildings using Statistical Energy Analysis*, Cambridge University Press, UK, 1996
- [3] A. Charpentier, D. Blanchet and K. Fukui, “Full Vehicle SEA Model Uses Detailed Sound Package Definition To Predict Driver’s Headspace Acoustic Response”, *Proc. INTER-NOISE 2004*, Prague, Czech Republic, 22-25 August 2004
- [4] M.C. Gomperts, “The sound insulation of circular and slit-shaped apertures”, *Acustica* **14**, 1-16 (1964)
- [5] P.J. Shorter and R.S. Langley, “Vibro-acoustic analysis of complex systems”, *J. Sound Vib.* **288**(3), 669-700 (2005)
- [6] V. Cotoni, P.J. Shorter and R.S. Langley, “Numerical and experimental validation of a finite element – statistical energy analysis method”, *J. Acoust. Soc. Am.*, **122**(1), 259-270 (2007)
- [7] VA One 2010, © The ESI Group, www.esi-group.com
- [8] N. Atalla, R. Panneton and P. Debergue, “A mixed pressure-displacement formulation for poroelastic materials” *J. Acoust. Soc. Am.*, **104**(3), 1444-1452 (1998)
- [9] J. Cordioli, V. Cotoni and P. Shorter, “Numerical investigation of the transmission loss of seals and slits for airborne SEA predictions”, *Proc. SAE NVH Conference*, 19-21 May 2009, St Charles, Illinois, USA, SAE 2009-01-2205
- [10] P.J. Shorter and R.S. Langley, “On the reciprocity relationship between direct field radiation and diffuse reverberant loading”, *J. Acoust. Soc. Am.*, **117**(1), 85-95 (2005)